Available online at www.sciencedirect.com
SCIENCE DIRECT®
Chaos, Solitons and Fractals 25 (2005) 287–298
CHAOS SOLITONS & FRACTALS
www.elsevier.com/locate/chaos

Numerical study of traveling-wave solutions for the Camassa–Holm equation

Henrik Kalisch [a,*], Jonatan Lenells [b]

[a] Department of Mathematics, NTNU, 7491 Trondheim, Norway
[b] Department of Mathematics, Lund University, 221 00 Lund, Sweden

Accepted 23 November 2004

Abstract

We explore numerically different aspects of periodic traveling-wave solutions of the Camassa–Holm equation. In particular, the time evolution of some recently found new traveling-wave solutions and the interaction of peaked and cusped waves is studied.

1. Introduction

The Camassa–Holm equation

$$u_t - u_{txx} + 3uu_x + 2\omega u_x = 2u_x u_{xx} + uu_{xxx}, \quad x \in \mathbb{R},\ t > 0, \tag{1.1}$$

arises as a model for the unidirectional propagation of shallow water waves over a flat bottom, $u(x,t)$ representing the water's free surface in non-dimensional variables, and ω being a constant related to the critical shallow water speed. Equation (1.1) was first obtained in [19] as an abstract bi-Hamiltonian equation with infinitely many conservation laws, and was subsequently derived from physical principles [2]. For a discussion of the physical relevance of (1.1) in the context of water waves we refer to [20]. In another context, (1.1) is a re-expression of the geodesic flow in the group of compressible diffeomorphisms of the circle [10,11,29]. Let us also point out that for a large class of initial data, Eq. (1.1) is an infinite-dimensional completely integrable Hamiltonian system: for the periodic case see [4,12], and for aspects of the direct/inverse scattering see [1,5,23]. Furthermore, the smooth solitary waves of (1.1) are solitons [16,21]. The Camassa–Holm equation models wave breaking [2,3,6,8,9,17,28,30] and admits wave solutions that exist indefinitely in time [3,7,8].

It was observed in [2] that Eq. (1.1), in addition to smooth waves, also admits peaked traveling-wave solutions (peakons)—see Fig. 1(c) and (d). Subsequently, it was observed through phase-plane analysis (see [27]) that also cusped waves exist—see Fig. 1(e) and (f). These non-smooth waves are weak solutions in the sense of Eq. (2.2) (see [26]).

Recently, a classification of the traveling-wave solutions of (2.2) was provided in [26], and it was found that a new peculiar class of weak traveling-wave solutions is obtained by combining cusps and peaks into traveling waves—see

* Corresponding author.
E-mail addresses: kalisch@math.ntnu.no (H. Kalisch), jonatan@maths.lth.se (J. Lenells).

0960-0779/$ - see front matter © 2005 Elsevier Ltd. All rights reserved.
doi:10.1016/j.chaos.2004.11.024

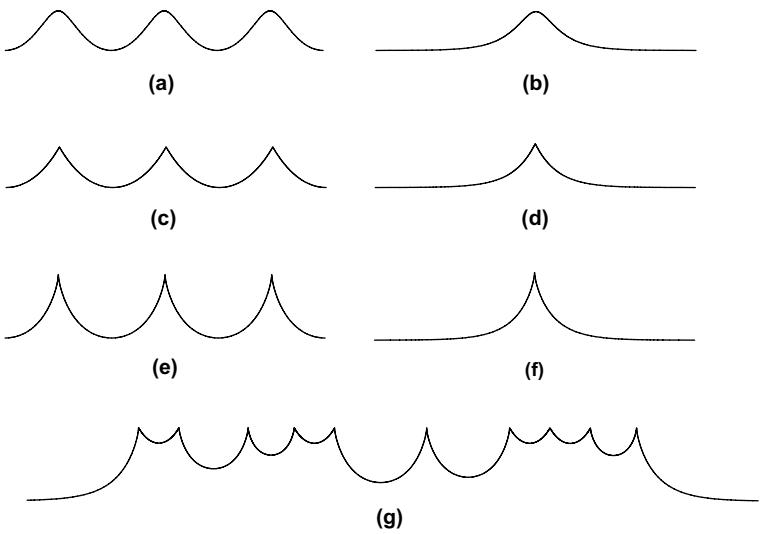

Fig. 1. Traveling-wave solutions of the Camassa–Holm equation: (a) smooth periodic; (b) smooth with delay; (c) periodic peakon; (d) peakon with decay; (e) periodic cuspon; (f) cuspon with decay and (g) composite waves.

Fig. 1(g). However, even though these wave patterns are mathematical solutions of (1.1), the question arises whether they can actually be observed physically.

The orbital stability of the smooth solitary waves of (1.1) was proved in [16]. Moreover, the peaked solutions, whether solitary waves or periodic waves, are orbitally stable [14,15,24,25].

In this paper we investigate numerically different aspects of the periodic traveling-wave solutions. We explore the time evolution of peaked, cusped and composite traveling waves. Furthermore, the interaction of peakons and cuspons is examined. It turns out that the numerical scheme confirms that all wave patterns, even the more exotic ones, travel unchanged. This affirms the validity of the definition of weak solutions of equation (1.1) given in the next section. Additionally, our study indicates that the cuspons interact elastically—suggesting a degree of rigidity in their shapes.

In Section 2 some notation is reviewed. The numerical algorithm is explained in Section 3. In Sections 4 and 5 we present our main results.

2. Preliminaries

2.1. Periodic distributions

Let $\mathbb{S}$ be the circle of length 2π. All functions are assumed to be real-valued. $C^\infty(\mathbb{S})$ denotes the set of smooth functions on $\mathbb{S}$. We let $\mathscr{D}'(\mathbb{S})$ be the space of distributions on $\mathbb{S}$, i.e. continuous linear functionals on $C^\infty(\mathbb{S})$. If $f \in \mathscr{D}'(\mathbb{S})$, we write f_x for its distributional derivative defined by

$$\langle f_x, \psi\rangle = -\langle f, \psi_x\rangle, \quad \psi \in C^\infty(\mathbb{S}),$$

where $\langle\cdot,\cdot\rangle$is the pairing between $\mathscr{D}'(\mathbb{S})$ and $C^\infty(\mathbb{S})$.

We denote, for $s \in \mathbb{R}$, by $H^s(\mathbb{S})$ the space of $f \in \mathscr{D}'(\mathbb{S})$ such that

$$\|f\|_{H^s}^2 = \sum_{k=-\infty}^{\infty} (1+k^2)^s |\hat{f}(k)|^2 < \infty,$$

where the Fourier coefficients are defined by

$$\hat{f}(k) = \langle f, \exp(-ik\cdot)\rangle, \quad k \in \mathbb{Z}.$$

The Hilbert spaces $H^s(\mathbb{S})$ are endowed with the inner products

$$(f,g)_{H^s} = \sum_{k=-\infty}^{\infty} (1+k^2)^s \hat{f}(k)\bar{\hat{g}}(k).$$

2.2. Weak solutions and stability

The functionals

$$H_0[u] = \int_{\mathbb{S}} u\,\mathrm{d}x, \quad H_1[u] = \frac{1}{2}\int_{\mathbb{S}} (u^2 + u_x^2)\mathrm{d}x, \quad H_2[u] = \frac{1}{2}\int_{\mathbb{S}} (u^3 + uu_x^2 + 2\omega u^2)\mathrm{d}x \tag{2.1}$$

are formally conserved under the flow of the Camassa–Holm equation. Eq. (1.1) can be written as

$$u_t + \left(\frac{1}{2}u^2 + (1-\partial_x^2)^{-1}\left[u^2 + \frac{1}{2}u_x^2 + 2\omega u\right]\right)_x = 0. \tag{2.2}$$

Indeed, applying $(1-\partial_x^2)$ to both sides gives (1.1). Following [13], by a *solution of* (1.1) with initial data $u_0 \in H^1(\mathbb{S})$, we mean a function $u \in C([0,T), H^1(\mathbb{S}))$ such that $u(0) = u_0$, (2.2) holds in distributional sense, and the functionals H_0, H_1 and H_2 are conserved.

A traveling-wave solution $u(x,t) = \varphi(x-ct)$ of (1.1) is said to be *orbitally stable* if for every $\epsilon > 0$ there is a $\delta > 0$ such that if $v \in C([0,T); H^1(\mathbb{S}))$ is a solution to (1.1) with

$$\|v(\cdot,0) - \varphi\|_{H^1(\mathbb{S})} < \delta,$$

then

$$\inf_{\xi\in\mathbb{S}} \|v(\cdot,t) - \varphi(\cdot-\xi)\|_{H^1(\mathbb{S})} < \epsilon \quad \text{for } t \in (0,T).$$

Since $H^1(\mathbb{S}) \subset L^\infty(\mathbb{S})$, orbital stability ensures that the shape of the traveling wave is stable. Therefore the traveling wave is likely to be numerically observable.

We say that a continuous function φ has a *peak* at x if φ is smooth on either side of x and

$$0 \neq \lim_{y\uparrow x} \varphi_x(y) = -\lim_{y\downarrow x} \varphi_x(y) \neq \pm\infty.$$

Wave profiles with peaks are called *peaked waves* or *peakons* (cf. [2,26]), indicating that they interact elastically.

Similarly, a continuous function φ is said to have a *cusp* at x if φ is smooth locally on both sides of x and

$$\lim_{y\uparrow x} \varphi_x(y) = -\lim_{y\downarrow x} \varphi_x(y) = \pm\infty.$$

We will call waves with cusps *cusped waves* or *cuspons*.

3. Numerical algorithm

The numerical simulations of Eq. (1.1) are carried out by means of a pseudospectral scheme. In order to explain the approach we assume $u(x,t)$ to be a solution of (1.1) with period L. We let $v \in C([0,T), H^1(\mathbb{S}))$ be the scaled function

$$v(x,t) = \frac{1}{a}u(ax,t), \quad x \in \mathbb{S},\ t \in [0,T),$$

where $a = \frac{L}{2\pi}$. Then v satisfies

$$a^2 v_t - v_{txx} + 3a^2 v v_x + 2a\omega v_x = 2v_x v_{xx} + v v_{xxx}.$$

We rewrite this as

$$a^2 v_t - v_{txx} = \left(-2a\omega v - \frac{3}{2}a^2 v^2 + \frac{1}{2}(v^2)_{xx} - \frac{1}{2}v_x^2\right)_x.$$

Applying the Fourier transform, we get

$$(a^2 + k^2)\hat{v}_t = \frac{\mathrm{i}k}{2}\left(-4a\omega\hat{v} - 3a^2\widehat{v^2} - k^2\widehat{v^2} - \widehat{v_x^2}\right), \tag{3.1}$$

which can be written as

$$\hat{v}_t = F(\hat{v}), \tag{3.2}$$

where

$$F(\hat{v}) = \frac{ik}{2(a^2+k^2)}(-4a\omega\hat{v} - 3a^2\widehat{v^2} - k^2\widehat{v^2} - \widehat{v_x^2}). \tag{3.3}$$

If the wave profile $v(\cdot,t)$ is known at a particular time t, an explicit four-stage Runge–Kutta method is adopted to compute $v(\cdot,t+h)$. More explicitly, we let

$$\begin{aligned}
V_1 &= \hat{v}(\cdot,t), \quad \Gamma_1 = F(V_1),\\
V_2 &= V_1 + \frac{h}{2}\Gamma_1, \quad \Gamma_2 = F(V_2),\\
V_3 &= V_2 + \frac{h}{2}\Gamma_2, \quad \Gamma_3 = F(V_3),\\
V_4 &= V_3 + h\Gamma_3, \quad \Gamma_4 = F(V_4).
\end{aligned}$$

Finally, these functions are combined to yield

$$\hat{v}(\cdot,t+h) = \hat{v}(\cdot,t) + \frac{h}{6}(\Gamma_1 + 2\Gamma_2 + 2\Gamma_3 + \Gamma_4).$$

This scheme is formally fourth-order convergent. That is, for smooth functions, decreasing the time step by a factor of 2 will lower the error by a factor of 16.

In the numerical implementation, a finite number N ($N = 2^n$ for some $n \in \mathbb{N}$) of spatial grid points $x_j = \frac{2\pi j}{N}$, $j = 0, 1, \ldots, N-1$, are used to approximate functions. The discrete Fourier transform of a function $v : \mathbb{S} \to \mathbb{R}$ is defined by

$$\hat{v}(k) = \frac{1}{N}\sum_{j=0}^{N-1} v(x_j)\mathrm{e}^{-\mathrm{i}kx_j}, \quad k = -\frac{N}{2}+1, \ldots, \frac{N}{2}.$$

The inverse Fourier transform is

$$V_N(x) = \sum_{k=-N/2+1}^{N/2} \hat{v}(k)\mathrm{e}^{\mathrm{i}kx}, \quad x \in \mathbb{S}.$$

Note that this is an exact expression at the grid points:

$$V_N(x_m) = \frac{1}{N}\sum_{k=-N/2+1}^{N/2}\sum_{j=0}^{N-1} v(x_j)\mathrm{e}^{\mathrm{i}k2\pi(m-j)/N} = v(x_m), \quad 0 \leqslant m \leqslant N-1.$$

Derivatives are computed as

$$v_x(x) = \sum_{k=-N/2+1}^{N/2} ik\hat{v}(k)\mathrm{e}^{\mathrm{i}kx}, \quad x \in \mathbb{S}.$$

To validate the code we examine the functionals H_i, $i = 0, 1, 2$, given in (2.1), which ought to be conserved with time. For a fixed time $T > 0$ and initial data $u(\cdot,0)$, let $u(\cdot,T)$ be the wave at time T obtained via the numerical algorithm. We are interested in the convergence of $|H_i[u(\cdot,T)] - H_i[u(\cdot,0)]|$ due to the space and time discretization. For initial data $u(x,0) = \sin(x)$, period $L = 2\pi$, and $T = 1$ we get the results presented in Table 1, which shows that these errors go down at a definite rate.

Table 1
Conservation of the functionals H_i, $i = 0,1,2$

N	h	H_0-error	Ratio	H_1-error	Ratio	H_2-error	Ratio
2^8	2^{-8}	7.92e−4		2.20e−2		5.81e−4	
2^9	2^{-9}	1.98e−4	4.00	1.08e−2	2.03	1.45e−4	4.02
2^{10}	2^{-10}	4.95e−5	4.00	5.42e−3	2.00	3.61e−5	4.00
2^{11}	2^{-11}	1.24e−5	4.00	2.71e−3	2.00	9.04e−6	4.00
2^{12}	2^{-12}	3.10e−6	4.00	1.35e−3	2.00	2.26e−6	4.00

4. Numerical results—traveling-wave solutions

In this section, we investigate numerically the different kinds of traveling-wave solutions for the Camassa–Holm equation. The experiments are carried out as follows. For given initial data $\varphi(\cdot) = u(\cdot, 0)$ and a fixed $T > 0$ we compare the wave $u(\cdot, T)$ obtained by the numerical algorithm with the translated wave $\varphi(\cdot - cT)$. Decreasing the time step h and increasing the number of spatial grid points N, we investigate the convergence of the L^2- and L^∞-errors.

We will henceforth assume $\omega = 0$. Moreover, all simulations are performed with speed $c = 1$. The statements concerning traveling waves of (1.1) can be found in [26].

4.1. Smooth traveling waves

To describe the traveling waves we use three parameters $m, M, z \in \mathbb{R}$, where $z = c - M - m$. If $z < m < M < c$, then there is a smooth periodic traveling wave $\varphi(x - ct)$ of (1.1) with $m = \min_{x\in\mathbb{R}}\varphi(x)$ and $M = \max_{x\in\mathbb{R}}\varphi(x)$, given implicitly by

$$|x - x_0| = \int_{\varphi_0}^{\varphi} \frac{\sqrt{c-y}}{\sqrt{(M-y)(y-m)(y-z)}}\,\mathrm{d}y, \tag{4.1}$$

where $\varphi(x_0) = \varphi_0$. This integral has singularities at $y = m$ and $y = M$. However, the change of variables

$$\varphi = m + (M - m)\sin^2\theta$$

transforms (4.1) into

$$|x - x_0| = 2\int_{\theta_0}^{\theta} \frac{\sqrt{A - \sin^2 t}}{\sqrt{B + \sin^2 t}}\,\mathrm{d}t, \tag{4.2}$$

where

$$A = \frac{c-m}{M-m} \quad \text{and} \quad B = \frac{m-z}{M-m}. \tag{4.3}$$

Since $B > 0$, (4.2) supplies a numerically more convenient expression for the traveling waves. To construct initial data we use (4.2) to compute $x(\varphi_j)$ for a dense grid of φ_j's. Performing a spline interpolation we obtain φ as a function of x.

We study a smooth periodic traveling wave with $m = 0.3$ and $M = 0.7$. This wave has period $L \approx 6.56$. We choose $T = L/4$ and $h = 0.0005 \cdot T$. The error due to spatial discretization decreases quickly as the number of grid points N is increased (see Table 2). If we instead keep $N = 128$ fixed and decrease the time step we get the result shown in Table 3.

Table 2
For the smooth traveling wave with $m = 0.3$, $M = 0.7$, and $c = 1$, the error due to spatial discretization decreases spectrally as the number of grid points N is increased

N	L^2-error	Ratio
8	7.45e−3	
16	9.00e−5	82.81
32	8.32e−8	1082.04
64	3.64e−9	22.83
128	3.65e−9	1.00

Table 3
The error decreases as $h \to 0$ for the smooth periodic traveling wave with $m = 0.3$, $M = 0.7$, and $c = 1$. The formal ratio of 16 is approximately achieved for the first three calculations

h	L^∞-error	Ratio
0.075	2.77e−6	
$0.075 \cdot 2^{-1}$	1.53e−7	18.04
$0.075 \cdot 2^{-2}$	1.37e−8	11.21
$0.075 \cdot 2^{-3}$	2.21e−8	0.62
$0.075 \cdot 2^{-4}$	2.27e−8	0.97

Thanks to the smoothness of the wave, we observe convergence close to the expected rate in both cases until the error due to other factors is reached.

4.2. Cusped traveling waves

Whenever $z < m < c < M$, there is a cusped periodic traveling wave $\varphi(x - ct)$ of (1.1) given implicitly by (4.1) with $m = \min_{x\in\mathbb{R}}\varphi(x)$ and $c = \max_{x\in\mathbb{R}}\varphi(x)$. Again we make the change of variables

$$\varphi = m + (M - m)\sin^2\theta,$$

and find

$$|x - x_0| = 2\int_{\theta_0}^{\theta} \frac{\sqrt{A - \sin^2 t}}{\sqrt{B + \sin^2 t}}\,\mathrm{d}t,$$

where A and B are given by (4.3). Note that this time θ ranges only from 0 to $\arcsin(\sqrt{A}) < \frac{\pi}{2}$. Locally at its crest a cuspon behaves like (see [26])

$$\varphi(x) = c - \alpha|x - x_0|^{2/3} + \mathrm{O}((x - x_0)^{4/3}) \quad \text{as } x \to x_0 \tag{4.4}$$

for some constant $\alpha > 0$.

Since the cuspons have singularities at their crests, it is to be expected that a large number of grid points need to be used in their numerical simulation. For our experiment (Fig. 2) we choose $m = 0$ and $M = 1.1$, which gives $L \approx 6.89$. For $T = L/4$ and $h = 0.0001 \cdot T$, Table 4 shows the convergence due to increasing N. The order of convergence appears to be approximately 0.67. This value will be explained further momentarily.

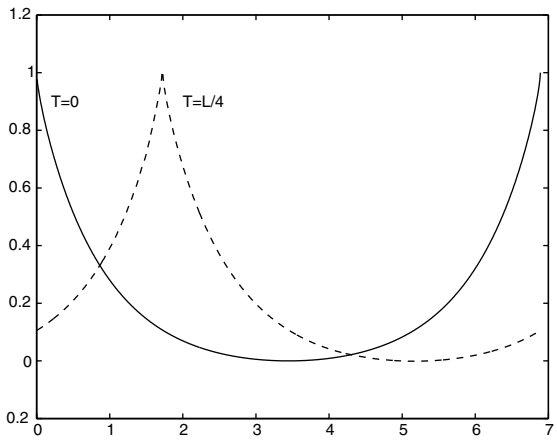

Fig. 2. The cusped traveling wave with $m = 0$, $M = 1.1$, and $c = 1$ displayed at time zero (solid) and at time $T = L/4 \approx 1.72$ (dashed).

Table 4
Convergence of cusped wave with $m = 0$, $M = 1.1$, and $c = 1$

N	L^∞-error	Ratio
256	2.49e−2	
512	1.39e−2	1.79
1024	8.01e−3	1.73
2048	4.86e−3	1.65
4096	3.04e−3	1.60

4.3. Composite traveling waves

For any fixed $c \in \mathbb{R}$ and $a > -\frac{c^2}{3}$, the equation

$$a = -Mm - (M+m)(c-M-m), \tag{4.5}$$

describes an ellipse in the (m, M)-plane with center $(\frac{c}{3}, \frac{c}{3})$ and major axis in the direction $(1, -1)$. For any $(m, M) \in \{z \leqslant m < c \leqslant M\} \cup \{z \geqslant m > c \geqslant M\}$ there is a corresponding cuspon or peakon given implicitly by (4.1). A countable number of cuspons and peakons corresponding to points (m, M) that belong to the same ellipse, may be joined at their crests where $\varphi = c$, to form a composite wave φ. If the Lebesgue measure $\mu(\varphi^{-1}(c)) = 0$, then φ is a traveling wave of (1.1).

To construct a composite wave, assume that the first cusp has parameters (m_1, M_1). From (4.5) we find the corresponding a. Solving for M in (4.5) yields

$$M = \frac{c-m}{2} + \frac{1}{2}\sqrt{c^2 + 2mc - 3m^2 + 4a}. \tag{4.6}$$

Thus, if the minimum m_2 of the second cuspon is given, M_2 defined by (4.6) will give a point on the same ellipse.

Table 5 shows the data obtained for a composite wave traveling at speed $c = 1$ consisting of two cuspons with $m_1 \approx 0.71$, $M_1 = 3$, $m_2 = 0.5$, and M_2 given by (4.6). Here m_1 is chosen so that the two crests of the initial data are situated at $x = 0$ and $x = \frac{3}{8}L$. This way there will always be a grid point at the very top, which gives a more even convergence. In the simulation $L \approx 0.88$, $T = L/8$, and $h = 0.0005 \cdot T$ (see Fig. 3).

The importance of the constant a in the construction of the composite waves is easily seen numerically. When two cuspons or peakons corresponding to different ellipses are joined into a traveling wave, one crest rises while the other one subsides. A balance is struck only for equal a's.

Admittedly, the error for the cusped and composite waves converges rather slowly to zero, albeit at a definite rate. One way of understanding the rate of convergence is as follows. A glance at the magnified picture of the crest in Fig. 3, shows that the error is due to the left one of the two grid points at the top. If x_0 is the position of the cusp, it is therefore reasonable to expect the L^∞-error to decrease like $E(N) = c - \varphi(x_0 - \Delta x)$ as $N \to \infty$ where $\Delta x = \frac{2\pi}{N}$. In view of the asymptotic formula (4.4) we have

Table 5
Error due to spatial discretization of a composite traveling wave with two cusps

N	L^∞-error	Ratio
128	6.02e−2	
256	4.28e−2	1.41
512	2.96e−2	1.44
1024	2.00e−2	1.48
2048	1.13e−2	1.52

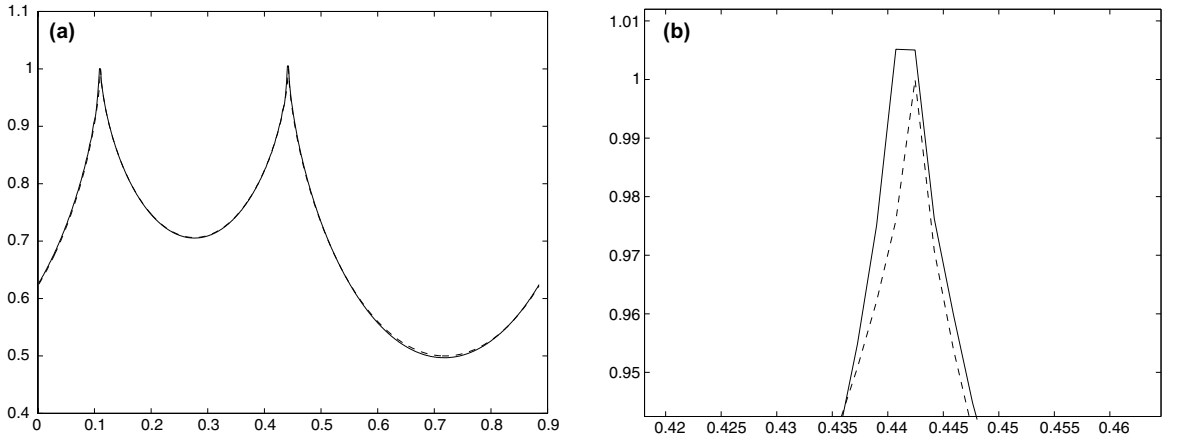

Fig. 3. The composite wave at time $T = L/8 \approx 0.11$, obtained via the numerical scheme (solid) and compared with the translated wave (dashed). The right picture is a close-up of the second cusp.

$$c - \varphi(x_0 - \Delta x) \approx \alpha|\Delta x|^{2/3} \quad \text{as } \Delta x \to 0$$

for some constant $\alpha > 0$. We infer that the expected ratio of convergence for the L^∞-error is

$$\frac{E(N)}{E(2N)} \approx \frac{\left(\frac{2\pi}{N}\right)^{2/3}}{\left(\frac{2\pi}{2N}\right)^{2/3}} = 2^{2/3} \approx 1.587.$$

This agrees well with the numbers shown in Tables 4 and 5.

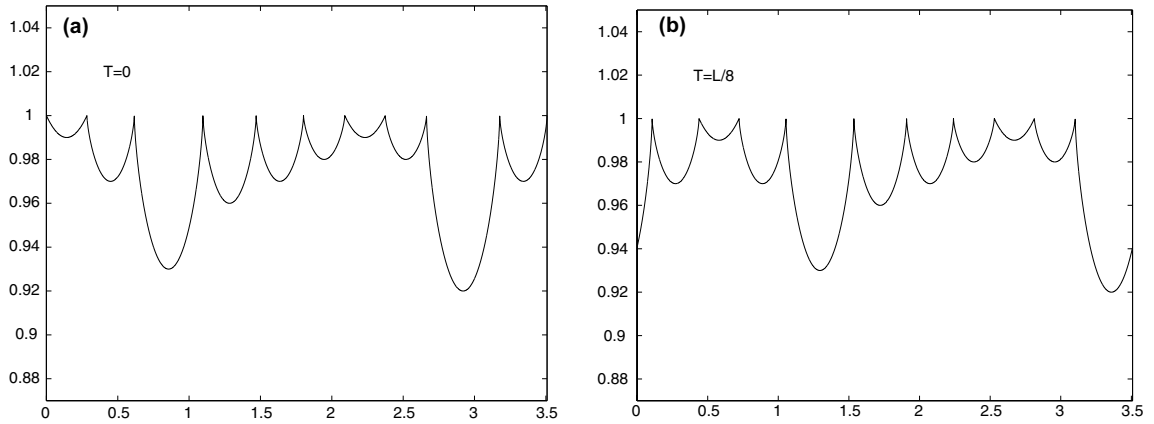

Fig. 4. Composite wave at time $T = 0$ and $T = L/8 \approx 0.44$. The first and seventh wave parts from the left are peakons; the other cuspons.

Table 6
Error due to spatial discretization of a composite traveling wave consisting of eight cuspons and two peakons

N	L^∞-error	Ratio
2^7	5.69e−3	
2^8	4.91e−3	1.16
2^9	3.39e−3	1.45
2^{10}	2.37e−3	1.43
2^{11}	1.90e−3	1.25
2^{12}	1.40e−3	1.35
2^{13}	8.88e−4	1.58
2^{14}	6.90e−4	1.29

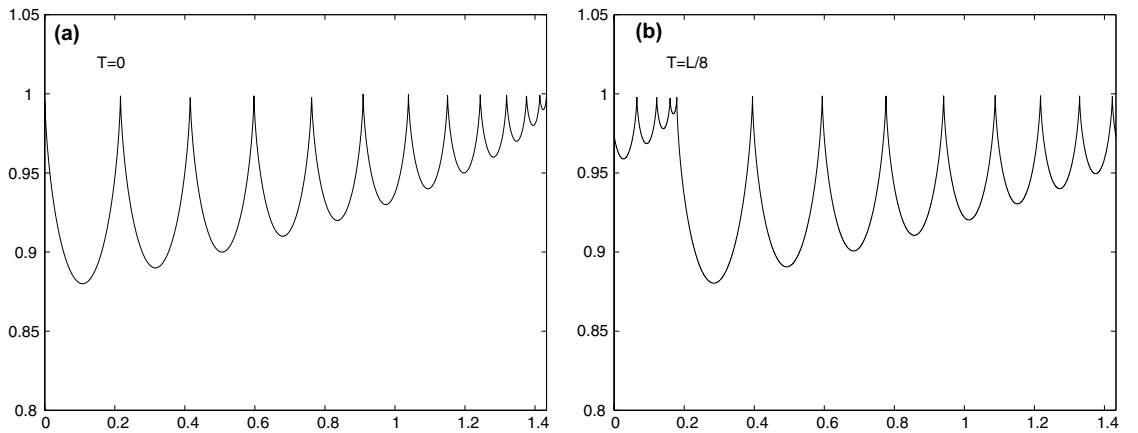

Fig. 5. Composite traveling wave—cuspons organized in a fractal pattern at times $T = 0$ and $T = L/8 \approx 0.18$.

To give another example, we construct a composite wave with eight cuspons and two peakons—see Fig. 4. The wave has period $L \approx 3.5$ and we choose $T = L/8$. We obtain results as shown in Table 6. The convergence is slightly uneven because some grid distributions match the positions of the crests better than others. Similarly, we can construct a composite wave with a fractal appearance as in Fig. 5.

5. Numerical results—interaction

In this section we explore the behavior of two interacting traveling waves of different sizes. Being an integrable equation, we anticipate the traveling waves of the Camassa–Holm equation to be solitons. Indeed, the smooth solitary waves of (1.1) have the spectral characteristics of solitons [16]. Moreover, in [2] it was found (see also [7]) that in the case of solitary waves, the two peakon interaction can be expressed as a Hamiltonian system. Indeed, the solution is

$$u(x,t) = p_1(t)\mathrm{e}^{-|x-q_1(t)|} + p_2(t)\mathrm{e}^{-|x-q_2(t)|}, \quad x,t \in \mathbb{R},$$

where the positions and heights of the two peaks evolve according to the Hamiltonian system

$$q_1' = p_1 + p_2\,\mathrm{e}^{-|q_1-q_2|}, \quad q_2' = p_1\,\mathrm{e}^{-|q_1-q_2|} + p_2,$$
$$p_1' = p_1p_2\,\mathrm{sign}(q_1-q_2)\mathrm{e}^{-|q_1-q_2|}, \quad p_2' = p_1p_2\,\mathrm{sign}(q_2-q_1)\mathrm{e}^{-|q_1-q_2|}.$$

Using an algebraic transformation of Eq. (1.1) into a deformed sinh-Gordon equation (see [22]), the interaction of cuspons was studied in [18]. Their results indicate clean interactions.

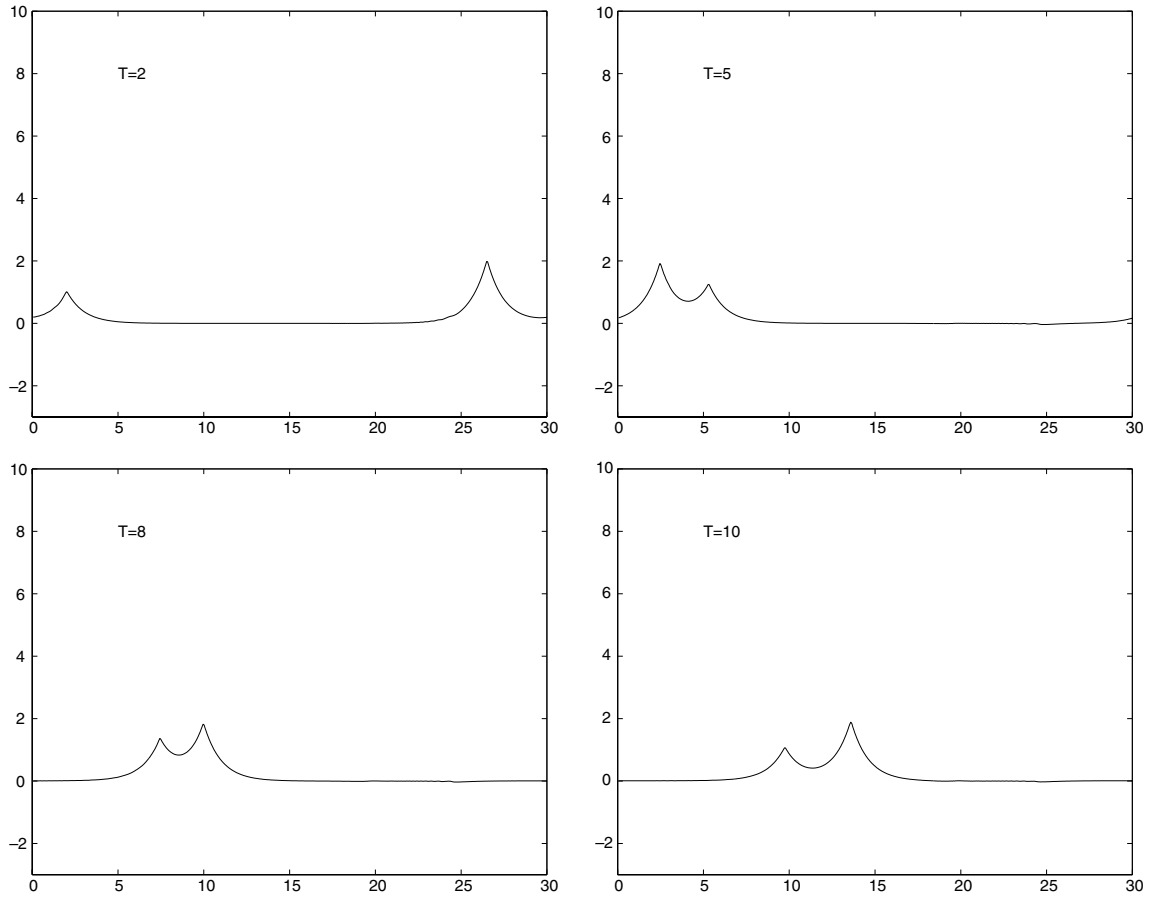

Fig. 6. Interaction of two peaked traveling waves.

It was proved in [26] that the traveling waves depend continuously on the parameters m and M in the H^1_{loc}-norm. In particular, this implies that a periodic traveling wave converges to the corresponding solitary wave as the period $L \to \infty$. Moreover, the solitary waves have exponential decay at infinity. Therefore, when investigating interaction of two traveling waves, we expect a simulation on a large interval to be a good approximation of the case of solitary waves.

On the other hand, whenever we approximate the evolution of a peakon or cuspon numerically, a small oscillatory tail is generated by the singularity at the crest after a certain number of time steps. As noticed in the previous section this error is due to the spatial discretization, and decreases at a definite rate as N is increased. However, this effect makes it disadvantageous to numerically integrate (1.1) over a long period of time for non-smooth initial data. Therefore, a

Table 7
Size of the dispersive tail generated by the interaction of two peakons

N	h	L^∞-norm	Ratio
2^8	$T \cdot 2^{-8}$	5.52e−2	
2^9	$T \cdot 2^{-9}$	2.62e−2	2.11
2^{10}	$T \cdot 2^{-10}$	1.42e−2	1.85
2^{11}	$T \cdot 2^{-11}$	7.96e−3	1.78
2^{12}	$T \cdot 2^{-12}$	4.58e−3	1.74
2^{13}	$T \cdot 2^{-13}$	2.65e−3	1.73

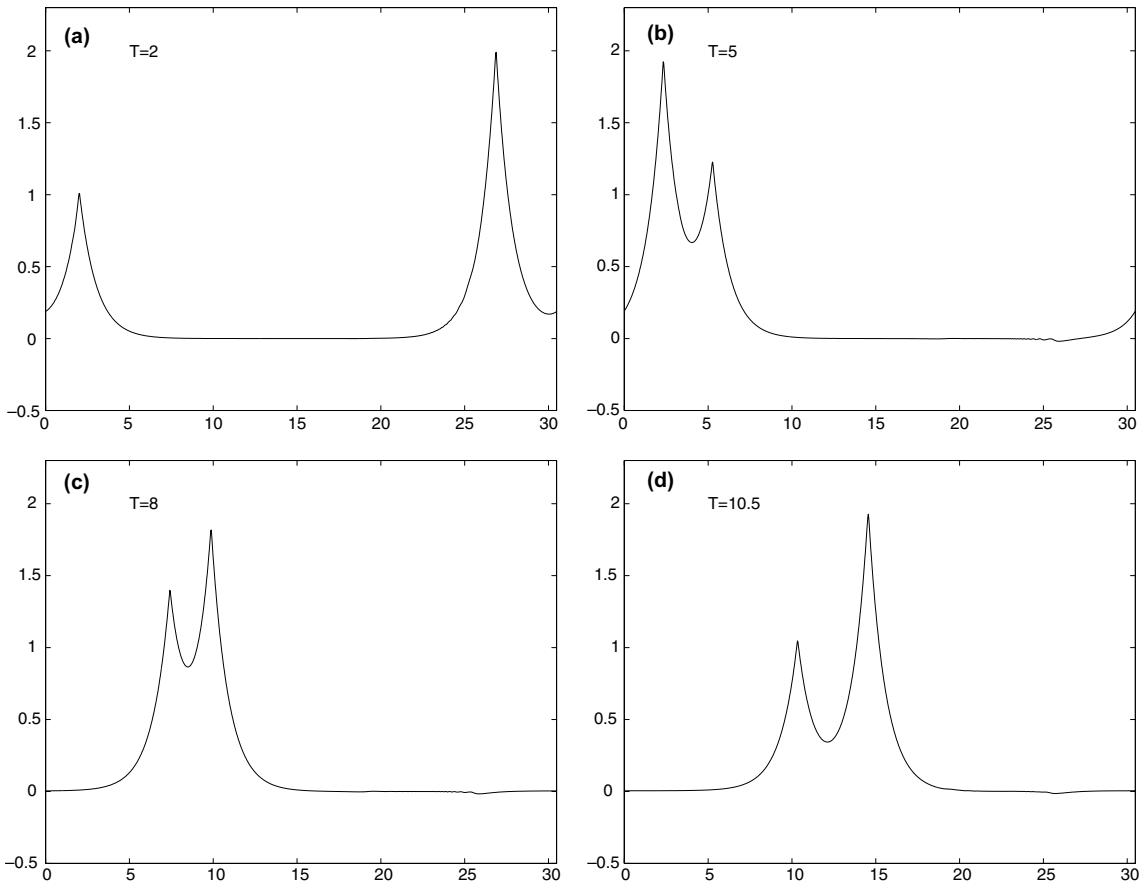

Fig. 7. Interaction of two cusped traveling waves.

very large initial separation of the two peakons or cuspons before their interaction introduces unnecessary complications.

In our study of interactions, we compromise and take a small enough initial separation, so that the singularities in the initial data do not affect the approximation before the interaction takes place.

5.1. Peakon interaction

The peakons are the only traveling waves for which there is a simple explicit formula. Indeed, for a given period L and speed c there is a unique peaked traveling-wave solution of the Camassa–Holm equation given by

$$\varphi(x) = \frac{c}{\cosh(L/2)} \cosh|x - x_0|, \quad |x - x_0| \leqslant L/2, \tag{5.1}$$

where x_0 is the position of the trough.

We take $L = 30$ and study the interaction of a peakon of height 2 with one of height 1, as shown in Fig. 6. As expected, the peakons exhibit a soliton-like behavior—the taller wave overtakes the shorter one, and afterwards both waves retain their original shapes. To ascertain a clean interaction we measure the size of the oscillatory tail generated by the interaction. In Table 7, the L^∞-norm of the dispersive tail is shown for different grid sizes, and it is apparent that the size of this tail decreases at a definite rate. Thus it is plausible that the dispersive tail is due to slight numerical instability in computations where the discretization is too coarse.

5.2. Cuspon interaction

To investigate the interaction of two cusped waves we take $m = 0$, $M = 1 + 10^{-6}$, $c = 1$, and use the implicit formula (4.1) to construct the corresponding cuspon. These values yield the period $L \approx 30.4$. Using the linear dependence of the traveling waves on the speed, viz. $\varphi_c = c\varphi_1$, we construct a translated wave of twice the size. After translating the cusp of

Table 8
Size of the oscillatory tail produced by the interaction of two cuspons

N	h	L^∞-error	Ratio
2^8	$T \cdot 2^{-8}$	6.75e−2	
2^9	$T \cdot 2^{-9}$	2.67e−2	2.53
2^{10}	$T \cdot 2^{-10}$	1.42e−2	1.89
2^{11}	$T \cdot 2^{-11}$	8.07e−3	1.76
2^{12}	$T \cdot 2^{-12}$	4.67e−3	1.73
2^{13}	$T \cdot 2^{-13}$	2.71e−3	1.72
2^{14}	$T \cdot 2^{-14}$	1.57e−3	1.73
2^{15}	$T \cdot 2^{-15}$	9.10e−4	1.72

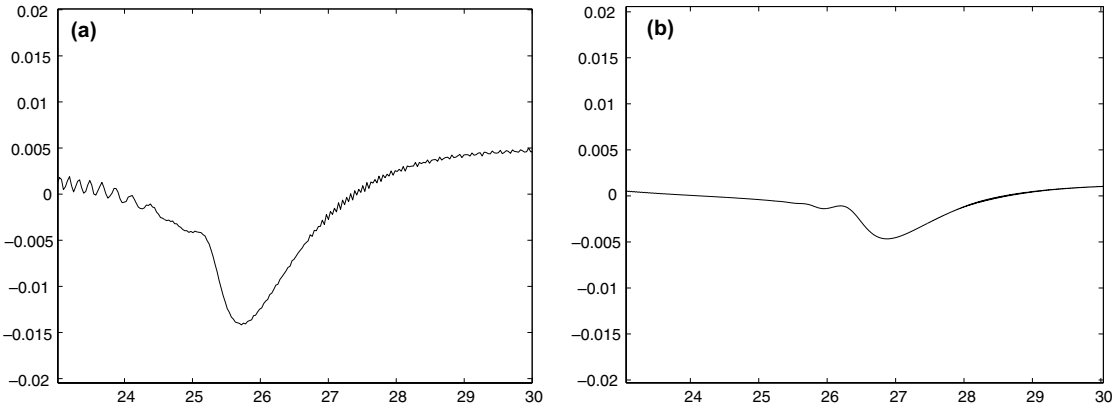

Fig. 8. Dispersive tail generated by the interaction of two cuspons for $N = 2^{10}$ and $h = T \cdot 2^{-10}$, respectively $N = 2^{12}$ and $h = T \cdot 2^{-12}$.

one of the two cuspons, they are then superimposed to yield the initial data. We obtain an interaction as shown in Fig. 7. Note that a small oscillatory tail is generated. However, just as for the peakon interaction, it is found that the size of the tail decreases at a definite rate as the grid is refined—see Table 8 and Fig. 8. The simulation therefore indicates an elastic interaction.

Acknowledgement

This work was supported in part by the BeMatA program of the Research Council of Norway.

References

[1] Beals R, Sattinger D, Szmigielski J. Acoustic scattering and the extended Korteweg–de Vries hierarchy. Adv Math 1998;40:190–206.
[2] Camassa R, Holm D. An integrable shallow water equation with peaked solitons. Phys Rev Lett 1993;71:1661–4.
[3] Constantin A. On the cauchy problem for the periodic Camassa–Holm equation. J Different Equat 1997;141:218–35.
[4] Constantin A. On the inverse spectral problem for the Camassa–Holm equation. J Funct Anal 1998;155:352–63.
[5] Constantin A. On the scattering problem for the Camassa–Holm equation. Proc R Soc London 2001;457:953–70.
[6] Constantin A, Escher J. Wave breaking for nonlinear nonlocal shallow water equations. Acta Math 1998;181:229–43.
[7] Constantin A, Escher J. Global existence and blow-up for a shallow water equation. Ann Sci Norm Sup Pisa 1998;26:303–28.
[8] Constantin A, Escher J. Well-posedness, global existence, and blowup phenomena for a periodic quasi-linear hyperbolic equation. Commun Pure Appl Math 1998;51:475–504.
[9] Constantin A, Escher J. On the blow-up rate and the blow-up set of breaking waves for a shallow water equation. Math Z 2000;233:75–91.
[10] Constantin A, Kolev B. On the geometric approach to the motion of inertial mechanical systems. J Phys A 2002;35:R51–79.
[11] Constantin A, Kolev B. Geodesic flow on the diffeomorphism group of the circle. Comment Math Helv 2003;78:787–804.
[12] Constantin A, McKean H. A shallow water equation on the circle. Commun Pure Appl Math 1999;52:949–82.
[13] Constantin A, Molinet L. Global weak solutions for a shallow water equation. Commun Math Phys 2000;211:45–61.
[14] Constantin A, Molinet L. Orbital stability of solitary waves for a shallow water equation. Phys D 2001;157:75–89.
[15] Constantin A, Strauss W. Stability of peakons. Commun Pure Appl Math 2000;53:603–10.
[16] Constantin A, Strauss W. Stability of the Camassa–Holm solitons. J Nonlinear Sci 2002;12:415–22.
[17] Danchin R. A few remarks on the Camassa–Holm equation. Differ Integral Equat 2001;14:953–88.
[18] Ferreira M, Kraenkel R, Zenchuk A. Soliton-cuspon interaction for the Camassa–Holm equation. J Phys A: Math Gen 1999;32:8665–70.
[19] Fuchssteiner B, Fokas A. Symplectic structures, their Bäcklund transformation and hereditary symmetries. Phys D 1981;4:47–66.
[20] Johnson R. Camassa–Holm, Korteweg–de Vries and related models for water waves. J Fluid Mech 2002;455:63–82.
[21] Johnson R. On solutions of the Camassa–Holm equation. Proc R Soc London A 2003;459:1687–708.
[22] Kraenkel R, Zenchuk A. Camassa–Holm equation: transformation to deformed sinh-Gordon equations, cuspon and soliton solutions. J Phys A: Math Gen 1999;32:4733–47.
[23] Lenells J. The scattering approach for the Camassa–Holm equation. J Nonlinear Math Phys 2002;9:389–93.
[24] Lenells J. Stability of periodic peakons. Int Math Res Notices 2004;10:485–99.
[25] Lenells J. A variational approach to the stability of periodic peakons. J Nonlinear Math Phys 2004;11:151–63.
[26] Lenells J, Traveling wave solutions of the Camassa–Holm equation. J Diff Eq, submitted.
[27] Li Y, Olver P. Convergence of solitary-wave solutions in a perturbed bi-Hamiltonian dynamical system. I. Compactons and peakons. Discrete Cont Dynam Syst 1997;3:419–32.
[28] Li Y, Olver P. Well-posedness and blow-up solutions for an integrable nonlinearly dispersive model wave equation. J Differ Eq 2000;162:27–63.
[29] Misiolek G. A shallow water equation as a geodesic flow on the Bott–Virasoro group. J Geom Phys 1998;24:203–8.
[30] McKean H. Breakdown of a shallow water equation. Asian J Math 1998;2:867–74.